Dynamic and Thermal Models for ECOSat-III

Sofia de Fátima Caeiro Aboobakar
sofia.caeiro@tecnico.ulisboa.pt

Instituto Superior Técnico, Universidade de Lisboa, Portugal

November 2016

Abstract

Launching a satellite into orbit is a demanding task from the point of view of maintaining the launcher's payload structural integrity and from the financial point of view. When it is decided to launch a satellite into orbit, its dynamic behaviour and its thermal profile during its orbit have to be maintained within specified levels to guarantee that no failure is caused by an inadequate structural and thermal design. Finite element models are used to predict the structure's behaviour. However, these models need to be validated by experimental tests. Validated models can be used with reliability to perform further simulations that allow to properly evaluate the satellite's behaviour and to correct it if needed. This task is harder when dealing with small satellites, the case of the ECOSat-III, a triple-unit CubeSat. This work describes the process of evaluating the behaviour of the satellite and performing its finite element model update using experimental data, whenever possible. The objective of this thesis is to increase the fundamental frequency of the nanosatellite and to make all its components operate in their safe temperature range by developing a thermal control system. The evaluation of the consequences of each design change has been performed and shows that with the proposed solutions, the ECOSat-III is ready to be launched and survive space environment conditions safely, from the structural and thermal point of views.

Keywords: Finite element model, Finite element model update, Fundamental frequency, Thermal control system, CubeSat

1. Introduction

The space industry plays an important role in society and the trend is to grow even further. The benefits of developing the space sector are not only for the advancement of science. The technology also improves the quality of life. Therefore, it is necessary to increase the awareness of these benefits, to motivate younger people to pursue a path in space industry and to develop the expertise to search for innovative solutions for complex problems. Since it is difficult to test space technologies in operating conditions, a careful modelling and analysis of all technical and design issues is necessary to increase the likelihood of success.

The ECOSat, the Enhanced Communications Satellite, is a nanosatellite designed by students at the University of Victoria as a response to the Canadian Satellite Design Challenge. Nanosatellites are satellites which dimensions and mass are very small when compared to typical satellites. NanoSats have 1 to 10 kg of mass [1]. The increase in the interest for this type of satellite and other smaller satellites is the shorter time to proceed from order to orbit (typically 10 to 12 months [2]) and the low cost of launching, since these satellites may be faced as a secondary payload. The ECOSat adopts a triple-CubeSat (triple cube satellite) configuration. It has dimensions of $10\times10\times34$ cm with a maximum mass of 4.0 kg [3]. The ECOSat-III has two primary missions: hyperspectral imaging of Canada and below-the-noise-floor communications system.

The main purpose of this thesis is to improve the mechanical design of the ECOSat-III satellite and to validate the structural and electrical components by means of dynamic and thermal analysis. To this end, a Finite Element Method model (FEM model) has been created based on the CAD model of the satellite. Modal analyses of the structure are performed in order to determine the lowest natural frequencies and the corresponding mode shapes of the satellite. Using the results from experimental testing conducted in David Florida Laboratory (DFL), experimental and numerical results are compared to update the FEM model, to obtain a more reliable FEM model. New configurations are studied and compared with the tested configuration. A solution is then proposed to increase the fundamental frequency to a value above the minimum required. Figure 1 shows the initial and final configuration of the satellite.

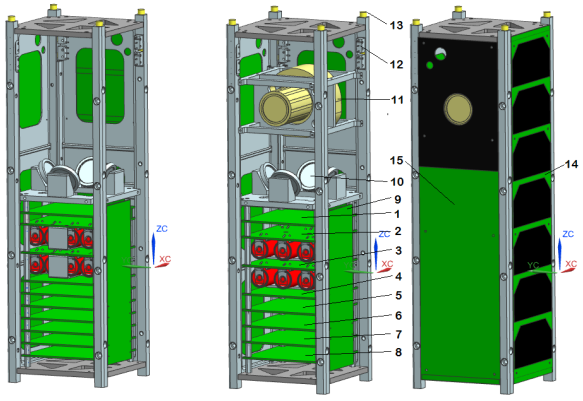

(a) Initial configuration

(b) Final configuration

Figure 1: Configurations before and after concluding subsystems design. Components: Connector (1), Battery (2, 3), Magnetorquers (4), GPS (5), OBC (6), Rx (7), Tx (8) boards, back plane (9), MWs (10), hyperspectral camera (11), deployment switches (12) and pins (13), solar panels (14) and antenna board (15)

With the dynamic behaviour corrected, thermal analyses are conducted by simulating the satellite's orbit to obtain the thermal cycling of the electronics stack and structural components. Different orbits are simulated with different power consumption profiles to identify hot case and cold case conditions, which represent worst case conditions. It is verified if all the components are within their safe temperature range. If they are not, a thermal control system is developed to put all the components working in their safe temperature range and reduce the temperature peaks and temperature deltas. In the end of this work, the satellite is dynamically and thermally prepared to survive launch and space environment conditions.

2. Theoretical Background

In this section, the historical and theoretical background and state of the art of the techniques used to model the vibration and thermal performance of the NanoSat structure and to perform experimental testing will be presented. The decisions taken and documented in subsequent sections are based in the theoretical background presented in this section.

2.1. Dynamic Analysis

2.1.1 Numerical Modal Analysis

Modal analysis of a structure allows to evaluate its natural modes of vibration and its natural frequencies, the frequencies at which each mode of vibration is excited. The first of the natural frequencies of a structure is called fundamental frequency. The physical parameters that most influence these modal parameters are the magnitude and distribution of masses and inertia, the elastic properties and the boundary conditions. The equations of motion of a multi degree of freedom system can be represented in matrix form as follows [4]:

$$\mathbf{M}\ddot{\mathbf{x}} + \mathbf{C}\dot{\mathbf{x}} + \mathbf{K_e}\mathbf{x} = \mathbf{f} \tag{1}$$

Since one wants to compute the natural frequencies and modes of vibration, there is no force applied to the structure. In the undamped case:

$$\mathbf{M}\ddot{\mathbf{x}} + \mathbf{K_e}\mathbf{x} = \mathbf{0} \tag{2}$$

Assuming a harmonic solution:

$$\mathbf{x} = \boldsymbol{\phi}\sin(\omega t + \varphi) \tag{3}$$

Substituting in Equation 2, a eigenvalue problem is obtained:

$$(\mathbf{K_e} - \omega^2\mathbf{M})\boldsymbol{\phi} = \mathbf{0} \tag{4}$$

A non-trivial solution for the eigenvalue problem is:

$$\det(\mathbf{K_e} - \omega^2\mathbf{M}) = \mathbf{0} \tag{5}$$

The eigenvectors $\boldsymbol{\phi}$ represent the modes of vibration of the structure. Obtaining the eigenvalues ω^2, the natural frequencies, in Hz, are:

$$f_i = \frac{\omega_i}{2\pi} \tag{6}$$

If the structure presents damping, the frequency of damped vibration can be obtained from:

$$\omega_{d_i} = \sqrt{1 - \zeta_i^2}\,\omega_i \tag{7}$$

Where ζ is the modal damping ratio and is given by:

$$\zeta_i = \frac{c_i}{2m_i\omega_i} \tag{8}$$

c_i and m_i represent the damping and mass terms of the correspondent equation. An oscillatory motion results if $\zeta < 1$, which corresponds to the underdamped case. In that situation, the frequency of damped vibration is always lower than the natural frequency.

2.1.2 Experimental Modal Analysis

It is possible to obtain the resonance frequencies and modes of vibration of a structure using experimental techniques. Two types of tests can be performed: impact testing or shaker testing. In the first case, a hammer is used to excite the structure, in the second case, the satellite is mounted in a shaker table to excite the structure [5]. In both cases, the displacement, velocity or acceleration is measured in different points and the ratio between it and the input force is transformed to the frequency domain using Fast Fourier Transform (FTT) and frequency response functions (FRFs) are obtained. The FRFs analysed in this work result from acceleration measurements. In that case, the resonance frequencies are the peaks from the amplitude diagram of the FRF and the mode shape components are the peaks of its imaginary part.

2.1.3 Finite Element Model Update

Experimental tests provide backup and validation data that can be compared with the results obtained from Finite Element Analysis (FEA). It is common to find incompatibility between the experimental and numerical modal data sets. When this happens, Finite Element Model Update must be performed to obtain a more realistic and reliable FEM model. To perform a FEM model update, the target responses that the FEM model is intended to present and the parameters that can be changed to achieve those responses must be selected. To better evaluate the parameters that most influence the responses, a sensitivity analysis must be performed. Sensitivity analysis quantifies the rate of change of a response with respect to a change in a parameter [6]. The resulting quantities are called sensitivity coefficients and form the sensitivity matrix $\mathbf{S}$. They can be computed using differential analysis:

$$\mathbf{S}_{ij} = \frac{\partial \mathbf{R'}_{ii}}{\partial \mathbf{P'}_{jj}} \tag{9}$$

To compare sensitivity coefficients, they must be relative and normalized:

$$\mathbf{S_r} = \frac{\partial \mathbf{R'}_{ii}}{\partial \mathbf{P'}_{jj}} \mathbf{P'}_{jj} \tag{10}$$

$$\mathbf{S_n} = \mathbf{S_r} \mathbf{R'}_{ii}^{-1} \tag{11}$$

The relationship between the responses and parameters can be given by a Taylor series truncated after the first term, resulting:

$$\Delta \mathbf{R'} = \mathbf{S} \Delta \mathbf{P'} \tag{12}$$

The Bayesian estimation method is used to minimize the error between the predicted response by the FEM model and the experimental response. It takes into account the level of confidence in both the parameters ($\mathbf{W_P}$) and responses ($\mathbf{W_R}$):

$$Er = \Delta \mathbf{R'}^T \mathbf{W_R} \Delta \mathbf{R'} + \Delta \mathbf{P'}^T \mathbf{W_P} \Delta \mathbf{P'} \tag{13}$$

The FEM model update procedure consists in minimizing that error and makes use of the following algorithm:

$$\mathbf{P'_u} = \mathbf{P'_0} + \mathbf{G}(-\Delta \mathbf{R'}) \tag{14}$$

Where $\mathbf{P'_u}$ are the updated parameters, $\mathbf{P'_0}$ is the actual state of the parameters, $\Delta \mathbf{R'}$ is the difference between the predicted and the experimental responses and $\mathbf{G}$ is a gain matrix given by:

$$\mathbf{G} = \mathbf{W_P}^{-1} \mathbf{S}^T (\mathbf{W_R}^{-1} + \mathbf{S} \mathbf{W_P}^{-1} \mathbf{S}^T)^{-1} \tag{15}$$

2.2. Thermal Analysis

To properly estimate the temperature distribution in a structure, it is necessary to take into account all the energy exchanges that take place with the surroundings. In space, heat transfer by convection is negligible due to the atmosphere rarefaction. As for conduction and radiation, they take a very significant role in the heat balance. The net rate of heat transfer that enters or leaves a body is [7]:

$$\dot{Q}_{\text{net}} = \dot{Q}_{\text{in}} - \dot{Q}_{\text{out}} + \dot{Q}_{\text{generation}} \tag{16}$$

This heat rate determines the change of temperature in that body:

$$\dot{Q}_{\text{net}} = m c_p \dot{T} \tag{17}$$

The rate of heat transfer that enters a body orbiting Earth by radiation is divided in four contributions, according to the heat source: solar radiation, albedo (solar radiation reflected back to space by Earth), Earth infrared radiation and radiation from surrounding bodies. In the case of a satellite composed by different components, different portions of those components will be exposed to the incoming radiation. Each component will absorb different fractions of the incoming radiation according to the surface finishing and the material. The rate of heat transfer absorbed by a component j is given by:

$$\dot{Q}_{\substack{\text{solar} \\ \text{absorbed}}} = \alpha'_{\text{solar}} F_{\text{Sun-j}} A_{\text{Sun}} \dot{q}_{\text{solar}} \tag{18}$$

$$\dot{Q}_{\substack{\text{albedo} \\ \text{absorbed}}} = \alpha'_{\text{solar}} F_{\substack{\text{Earth-j} \\ \text{sunlit}}} A_{\text{Earth}} \dot{q}_{\text{albedo}} \tag{19}$$

$$\dot{Q}_{\substack{\text{infrared} \\ \text{absorbed}}} = \alpha'_{\text{infrared}} F_{\text{Earth-j}} A_{\text{Earth}} \dot{q}_{\text{infrared}} \tag{20}$$

$$\dot{Q}_{\substack{\text{surroundings} \\ \text{absorbed}}} = \alpha'_{\text{infrared}} \sum_i F_{ij} A_i \dot{q}_i \tag{21}$$

Where the heat fluxes are, considering Earth and the Sun as blackbodies, and considering that the radiation emitted by Earth is equal to the solar radiation absorbed:

$$\dot{q}_{\text{solar}} = \sigma T_{\text{Sun}}^4 \tag{22}$$

$$\dot{q}_{\text{albedo}} = \text{BA} F_{\text{Earth-Sun}} \dot{q}_{\text{solar}} \tag{23}$$

$$\dot{q}_{\text{infrared}} = \alpha'_{\text{solar}} F_{\text{Earth-Sun}} \dot{q}_{\text{solar}} \tag{24}$$

$$\dot{q}_i = \varepsilon_i \sigma T_i^4 \tag{25}$$

The view factor between two surfaces is:

$$F_{ij} = \frac{1}{A_i} \int_{A_i} \int_{A_j} \frac{\cos\theta_i \cos\theta_j}{\pi L^2} \, dA_i dA_j \tag{26}$$

The rate of heat transfer that leaves a body orbiting Earth by radiation is:

$$\dot{Q}_{\text{emitted}} = A_j \varepsilon_j \sigma T_j^4 \tag{27}$$

The rate of heat transfer that enters or leaves a body by conduction is:

$$\dot{Q}_{\text{conduction}} = -\sum_i \frac{T_j - T_i}{\frac{L_i}{k_i A} + R_j + \frac{L_j}{k_j A}} \tag{28}$$

The rate of heat generation by Joule Effect is:

$$\dot{Q}_{\text{generation}} = P_e = UI \tag{29}$$

In the above equations, the subscript i is used to refer to surrounding components.

3. Dynamic Analysis

To perform modal analyses in the satellite structure a FEA software was used. Siemens NX 9 was chosen and the solver NX NASTRAN with Solution 103 Real Eigenvalues was used. From the computational model of the satellite a mesh is created, the connections and contacts between components are created and the boundary conditions are applied.

3.1. Finite Element Analysis

The FEM model consists of 3D, 2D and 1D meshes. 2D meshes are the result of idealizing boards and plates (printed circuit boards and bottom and top plates) to surfaces and 1D meshes result of idealizing screws and standoffs to beams. 3D meshes are used in all other components. Two boundary conditions sets were implemented: satellite fixed along its rails and satellite fixed in its rail's bases. The first set represents the case where the satellite does not have any clearance between its rails and the deployer rails. The second case represents the case where clearance exists, being the satellite only constrained by the top and bottom faces of the deployer. The two sets produced similar results. This is explained by the fact that the rails do not have any contribution to the first mode of vibration of the satellite. The convergence analysis of the fundamental frequency is shown in Figure 2.

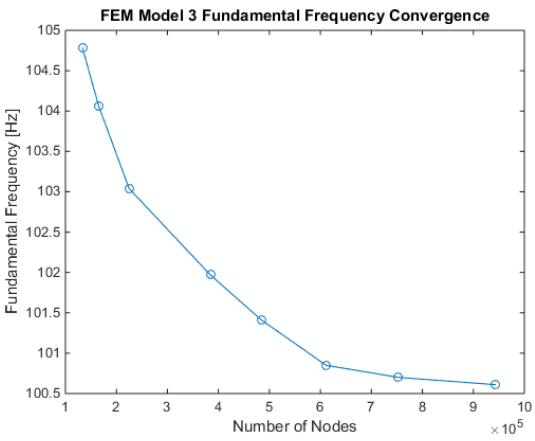

Figure 2: Convergence of the fundamental frequency for different FEM Models and boundary conditions.

With the last mesh used, the fundamental frequency was evaluated to be 100.6 Hz. The mesh used and the mode shape correspondent to the fundamental frequency is shown in Figure 3. To validate the result, it must be compared with experimental data.

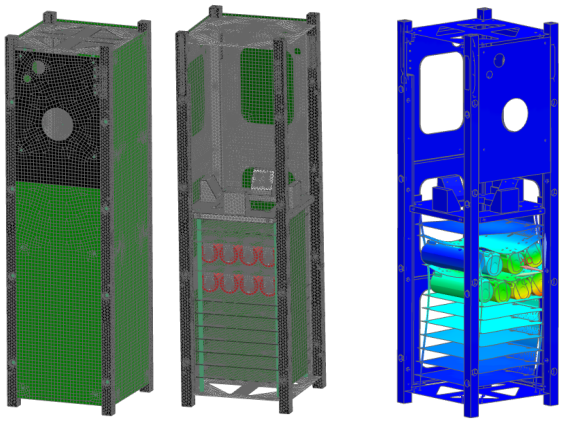

(a) FEM model mesh (b) First mode of vibration

Figure 3: Used mesh and obtained first mode of vibration

3.2. Experimental Modal Analysis Results

The experimental tests performed in DFL allowed to evaluate the fundamental frequency of the satellite to be located between 80 and 90 Hz, by analysing the FRF amplitude diagrams obtained. One of the diagrams with a peak in this range of frequencies is shown in Figure 4. Considering the

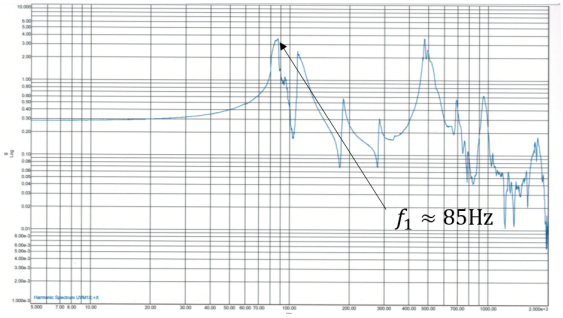

Figure 4: Fundamental frequency taken from the measurement of the accelerometer in the back plane

experimental fundamental frequency to be 85 Hz, the corresponding error of the FEM model is 18.4%. As for the mode shape, the information provided was incomplete as the FRF phase diagrams were not delivered to the ECOSat team. This represents a drawback, since one has to assume that the mode shape correspondent to the fundamental frequency is similar in both the computational model and the real model. However, the acceleration readings from the different accelerometers locations sustain evidence that the mode shape is the

same in both numerical and experimental results. The FRF amplitude diagram of the back plane is the one with a higher response between 80 and 90 Hz, which complies with the first mode of vibration being characterized by the significant deformation of this component. Therefore, it is concluded that the two fundamental frequencies obtained characterize the same mode shape. Because the difference between the two fundamental frequencies is significant and the real fundamental frequency is below 90 Hz, a FEM model update must be implemented before proposing a solution and evaluating it using the FEM model.

3.3. Finite Element Model Update

To perform FEM model update, the software FEMtools was chosen. The FEM model with the correspondent boundary conditions and the results from numerical and experimental modal analyses are imported. A correlation between the measuring points and the nodes of the FEM model and a correlation between the natural frequencies is performed. The target responses and the parameters to be changed to achieve them are selected. The model update is then performed. The FEM model update process was constrained by three factors:

- The type and quality of the experimental results. The testing results delivered were the FRF amplitude diagrams, in paper, without the associated electronic files generated by the software used. It was not possible to use signal processing to obtain accurate values for the natural frequencies (peaks of the FRF amplitude diagram) or information about damping (amplitude and width of the FRF peaks). Furthermore, the information about the mode shapes is incomplete (FRF phase diagrams were not delivered).
- Number of accelerometers used during testing. Only 6 sensors were used, each measuring only one degree of freedom. Although the information about their location is useful to obtain information about the mode shapes, it is not enough to correctly identify each mode.
- License used in FEMtools. The available license limited the FEM models used up to 50000 nodes. In the convergence study of FEM model 3, the most refined mesh has 943007 nodes while the most coarse mesh has 133529 nodes. This means that in order to be able to perform a FEM model update, the computational model must be even more simplified, which will increase the difference between the natural frequencies of the computational and real models.

Simplifying the FEM model, the new numerical fundamental frequency obtained is 110.3 Hz, with an error of 29.8% in the estimation of the fundamental frequency. The target responses were chosen to be the natural frequency and the real mass of the components which were possible to weight. The parameters to change to obtain those responses were geometric (shell thickness) and material properties (density, Young's modulus, shear modulus and Poisson's ratio). The sensitivity analysis in Figure 5 shows that the selected parameters have high sensitivity coefficients relative to the selected responses.

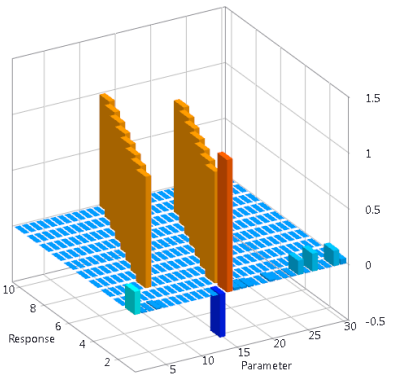

Figure 5: Sensitivity coefficients in graphic mode

Pairing the fundamental frequencies obtained and the nodes with the experimental measuring points, after 7 iterations, the FEM model update lead to a fundamental frequency of 97.2 Hz. Figure 6 shows the change in parameters and the responses evolution during the 7 iterations.

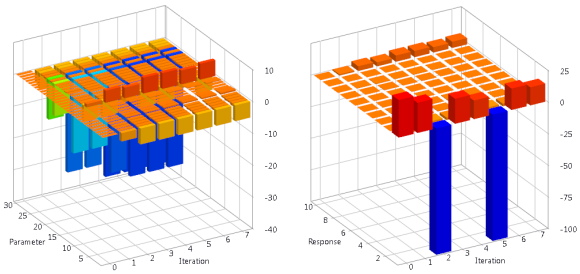

(a) Parameter changes (b) Response changes

Figure 6: Changes in the selected parameters and responses in each iteration of the updating process

Because the new result still presents a error of 14.4%, the parameter changes were applied to the refined mesh which had shown a fundamental frequency of 100.6 Hz. Applying the changes, the fundamental frequency changed to 87.1 Hz, which presents an error of 2.5%. This value is acceptable and the obtained FEM model is considered reliable.

3.4. New Configuration Modal Analysis

As mentioned in the Introduction, after experimental testing took place, some design changes were

made to the ECOSat-III. The effects on the fundamental frequency are evaluated to conclude if the satellite dynamic behaviour changes significantly. The number of printed circuit boards and batteries was changed (Model 2). Furthermore, another configuration was simulated. The remaining components of the satellite were mounted, meshed and the needed connections and contacts were defined (Model 3). Both new configurations were simulated with the initial parameter values and with the updated values. Table 1 shows the fundamental frequencies obtained. Figure 7 shows the mesh used for each of the new configurations tested. The mode shapes are similar to the previously obtained.

	Model 1	Model 2	Model 3
Before Update	100.6 Hz	99.8 Hz	97.1 Hz
After Update	87.1 Hz	86.0 Hz	83.4 Hz

Table 1: Fundamental frequencies of the three configurations

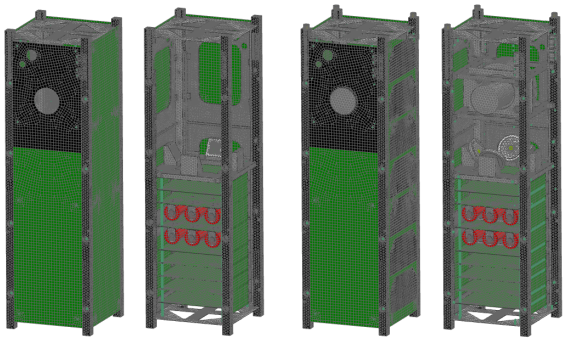

(a) Model 2 (b) Model 3

Figure 7: FEM Models with refined meshes

The corresponding deviation of the new updated models relative to the initial updated model is -1.3% and -4.2%, for Model 2 and Model 3, respectively. It can be concluded that these changes decrease the fundamental frequency of the satellite. Verifying the mode shapes, it can be concluded that they are the same in the three configurations. For these reasons, if the proposed solution increases the fundamental frequency of the satellite to a value above 90 Hz in Model 3, it will also increase it in Model 1 and Model 2.

3.5. Solution Development

To avoid going through a process of a major design change that would significantly modify the configuration of the satellite, it was decided to constrain the first mode of vibration. This way, the stiffness of this mode of vibration increases and so does the first natural frequency. The solution found was to add two small aluminum pieces, attach them to the side panel in the direction of the first mode of vibration and fix one of the PCBs with highest displacement. The location of the aluminum pieces is shown in Figure 8. This change increased

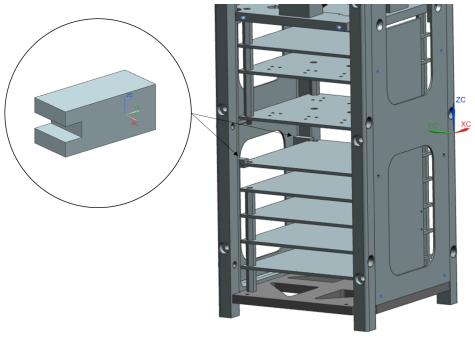

Figure 8: Aluminum stiffeners mounting

the fundamental frequency from 83.4 Hz to 130.6 Hz, meeting the requirements. The obtained mode shape is presented in Figure 9.

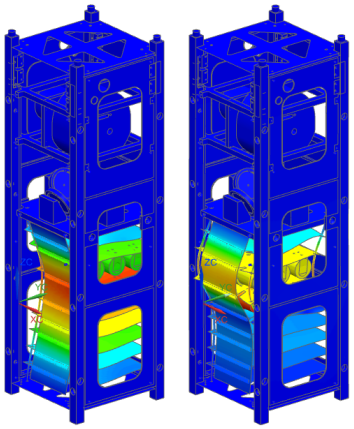

Figure 9: [First mode of vibration of the structure without (left) and with stiffeners (right)

4. Thermal Analysis

To perform thermal analyses, Siemens NX 9 was chosen and the solver NX SPACE SYSTEMS THERMAL was used. The mesh is created, the orbit, thermal loads and contacts between components are defined. Hot case and cold case conditions are identified and a thermal control system is developed to maintain all components within their safe temperature range.

4.1. Initial Finite Element Analysis

The FEM model consists of 3D and 2D meshes. 2D meshes are used in components with very low thickness like the solar cells. The remaining components, including the printed circuit boards, are meshed with 3D elements. 1D elements are not used in this FEM model.

As a simplification, only the external surfaces of the satellite are considered in the radiation ex-

change with the space environment. Other simplification is considering the thermal loads that should be applied in integrated circuits are applied to the whole printed circuit board area, since the integrated circuits were not modelled and mounted.

The convergence analysis of the temperature in three different nodes is presented in Figure 10. Convergence is not fully achieved but a trend is present. Due to computational resources, it was only possible to choose 12 orbital positions and 201002 nodes to perform the needed simulations.

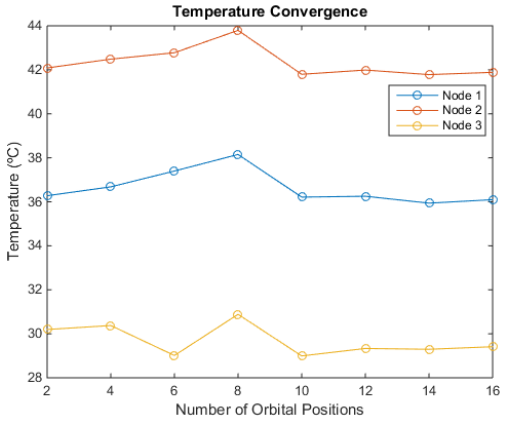

(a) Temperature convergence with number of orbital positions

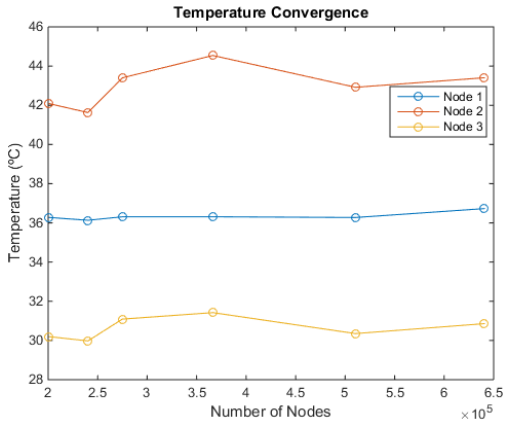

(b) Temperature convergence with number of nodes

Figure 10: Thermal analysis convergence study

Different orbits and different power consumption conditions are considered to identify the worst case conditions. To identify the hot case, full power consumption and Earth in perihelion position are used, to identify cold case, a reduced power consumption state and aphelion position are used. Table 2 shows the obtained results for each simulated orbit. Convergence was not fully achieved due to the high simulation times. Figure 11 shows the used mesh for thermal analysis.

It is verified that the hot case conditions are obtained for a satellite launched to a orbit of 600 km of altitude at 12 pm in perihelion and full power consumption, while cold case conditions are obtained for a satellite launched to a orbit of 800 km at 9 am in aphelion and reduced power consumption. In cold case conditions, the hyperspectral camera and the batteries fall to a temperature below their safe temperature range. The minimum safe temperature is 0°C, but the camera reaches -12.5°C and the batteries reach -2.4°C. For that reason, a thermal control system (TCS) must be implemented.

Altitude	Launch	Position	T_{max}	T_{min}
600 km	9 am	Aphelion	12.7	-17.41
		Perihelion	45.8	-9.1
	12 pm	Aphelion	29.3	-12.5
		Perihelion	62.8	-4.2
800 km	9 am	Aphelion	11.8	-17.4
		Perihelion	50.2	-7.6
	12 pm	Aphelion	28.3	-13.7
		Perihelion	62.5	-4.5

Table 2: Maximum and minimum temperatures in each simulated case (in °C)

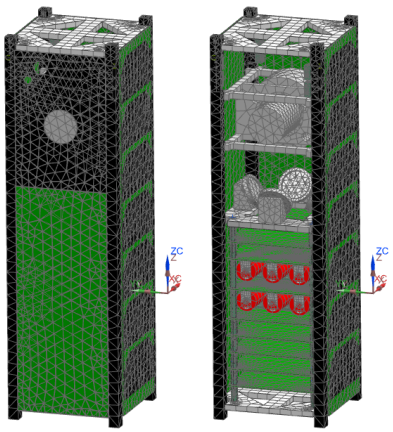

Figure 11: Thermal FEM Model

4.2. Thermal Control System

While passive systems are simple, highly reliable, lighter, cheaper and simple to implement, they have lower heat transfer capacity than active systems. Since the constraint of low mass, cost and limited power is an issue in NanoSats, passive thermal control systems are preferred. For this reason, a passive TCS will be implemented.

The first option consists in using black dye in the external surfaces to increase the absorptivity. This way, a bigger portion of radiation is absorbed by the satellite, and less is reflected, increasing the temperature of the components. This option allowed to increase the minimum temperatures, allowing the batteries to operate within their safe temperature range. As for the hyperspectral camera, its minimum temperature still remained below its safe tem-

perature range.

To increase the minimum temperature of the hyperspectral camera, one if its mounting plates material was changed to stainless steel, which presents a lower thermal conductivity than aluminum. Implementing this solution, the hyperspectral camera is allowed to operate in its safe temperature range.

The initial results (case 1), the results of applying black dye (case 2) and the results of changing the material of one camera mounting plate to stainless steel (case 3) are shown in Table 3.

Component	$T_{\min_1}$	$T_{\min_2}$	$T_{\min_3}$
Camera	-12.5	-1.0	5.5
Upper Batteries	-2.4	11.6	11.3
Lower Batteries	-0.6	13.3	13.1

Table 3: Minimum temperatures (in °C) of the components out of their safe temperature range and its evolution with the TCS implemented

With the TCS implemented, all the components operate within their safe temperature range in worst case conditions and in all intermediate conditions.

4.3. Additional Thermal Control System Improvement

Although all the components operate within their safe temperature range, reducing the temperature peaks and temperature deltas, the satellite's useful life can be improved. For that reason, further changes are proposed.

The proposed solution to achieve the desired result is to attach high thermal inertia plates to the electronics stack, where the temperature peaks and temperature deltas are higher, in hot case conditions. Different configurations were simulated: adding one, two or three plates with width of 40 or 60 mm, thickness of 3, 4 or 5 mm and made of aluminum, titanium or stainless steel. Analysing the different configurations the less beneficial ones are immediately excluded. The remaining solutions present different benefits. To choose the most beneficial one, an algorithm to attribute scores to each one was implemented:

- Select the maximum temperature, maximum temperature delta and maximum mass verified in the remaining options (56.40°C, 33.83°C and 0.465 kg respectively);
- Normalize the maximum temperatures, temperature deltas and mass, according to the maximum values from the previous step. The results are values between 0 and 1;
- Compute the average value of each solution option for each of the three tables. The results are values between 0 and 1;
- Compute the weighted average for each solution by assigning to each one of the parameters characterized by each table a weight that reflects their importance. Weights of 50%, 45% and 5% were assigned to the maximum temperature, temperature delta and mass, respectively. The low importance given to the mass is based on the fact that the heavier solutions were already excluded. The results are still between 0 and 1;
- Select the lowest result as the best solution.

Following this procedure, the chosen solution was to attach two stainless steel plates with width of 60 mm and thickness of 3 mm, with a total mass of 0.372 kg. This configuration is represented in Figure 12.

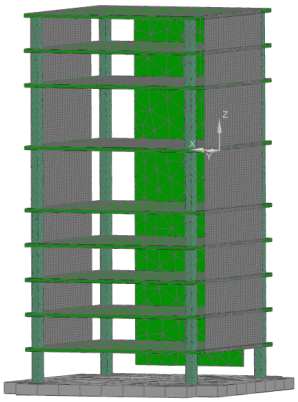

Figure 12: Proposed configuration to reduce maximum temperatures and temperature deltas (stainless steel plates on the sides and back plane in the back side)

Verifying the benefits of using stainless steel, the remaining camera mounting plates and the momentum wheel (MW) mounting plate were also changed to stainless steel. This allowed to reduce the temperature deltas in the components mounted in those plates. Tables 4, 5 and 6 show the results obtained in initial conditions (case 1), after applying black dye and stainless steel to one camera mount (case 3) and after attaching high thermal inertia plates and changing the remaining mounting plates to stainless steel (case 4). Each table presents a different parameter: minimum temperature reached in cold case conditions, maximum temperature achieved in hot case conditions and temperature delta in hot case conditions (temperature deltas are higher in hot case conditions).

The thermal cycling of the components is presented in Figure 13.

4.4. Fundamental Frequency Check

Because there was a change of material in some components and new components were added, a new vibration simulation is needed to verify that the fundamental frequency is still acceptable. The results are shown in Table 7. The centre of mass is in relation to the geometric centre of the satellite.

Component	$T_{\min_1}$	$T_{\min_3}$	$T_{\min_4}$
Camera	-12.5	5.5	15.2
MWs	-14.6	-6.2	-3.2
ACS Board	-14.6	-6.2	-1.0
Connector Board	-6.7	5.3	4.3
Battery Board 1	-3.1	10.5	8.2
Upper Batteries	-2.4	11.3	8.9
Battery Board 2	-1.1	12.5	9.7
Lower Batteries	-0.6	13.1	10.2
Magnetorquers Board	-8.1	3.2	4.8
GPS Board	-8.8	2.4	4.0
OBC Board	-8.2	2.7	3.8
Rx Board	-10.1	0.7	2.6
Tx Board	-10.9	-0.2	1.9
Structure	-15.0	-6.7	-6.3

Table 4: Minimum temperatures (in °C)

Component	$T_{\max_1}$	$T_{\max_3}$	$T_{\max_4}$
Camera	31.3	38.4	33.7
MWs	31.8	43.8	42.5
ACS Board	31.9	43.8	41.8
Connector Board	31.7	42.0	40.9
Battery Board 1	29.0	38.6	38.6
Upper Batteries	28.6	37.9	38.2
Battery Board 2	31.7	41.3	40.3
Lower Batteries	30.7	40.0	39.5
Magnetorquers Board	35.8	46.3	44.7
GPS Board	37.6	48.2	46.4
OBC Board	51.5	62.1	52.6
Rx Board	40.2	51.1	48.4
Tx Board	39.8	50.8	48.0
Structure	31.8	43.8	43.3

Table 5: Maximum temperatures (in °C)

Component	ΔT_1	ΔT_3	ΔT_4
Camera	29.1	24.1	7.5
MWs	33.5	42.4	38.5
ACS Board	33.3	41.9	34.6
Connector Board	19.1	24.5	24.9
Battery Board 1	10.8	14.1	17.2
Upper Batteries	9.4	12.2	16.1
Battery Board 2	11.1	14.4	16.5
Lower Batteries	9.4	12.2	15.3
Magnetorquers Board	23.5	30.2	25.9
GPS Board	24.4	31.4	27.1
OBC Board	25.4	32.7	28.4
Rx Board	26.8	34.4	29.9
Tx Board	28.2	36.1	31.4
Structure	33.5	42.0	40.6

Table 6: Temperature deltas (in °C)

Total mass	2.772 kg
Centre of mass	(0.03, -0.03, -4.35) mm
Fundamental frequency	248.7 Hz

Table 7: Fundamental frequency and solid properties after developing the TCS with all the mounting plates in stainless steel

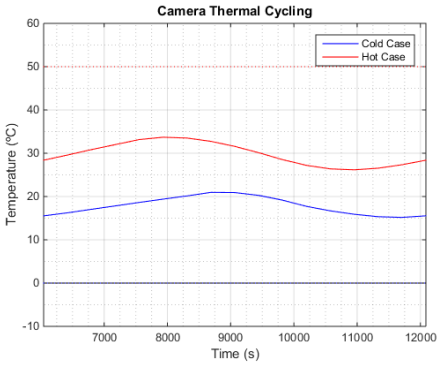

(a) Camera Thermal Cycling

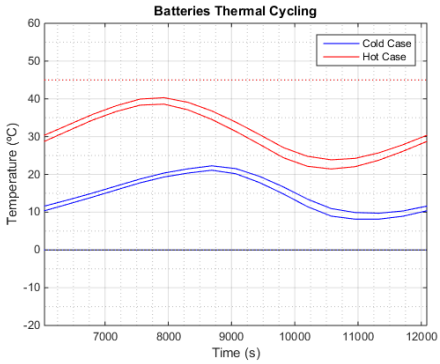

(b) Batteries Thermal Cycling

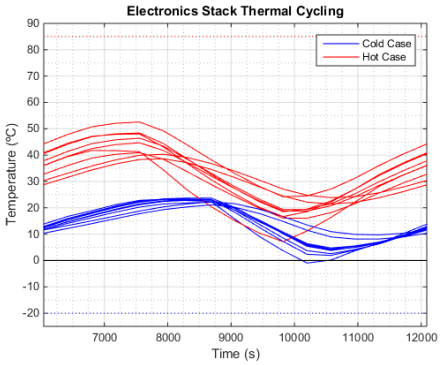

(c) Electronics Stack Thermal Cycling

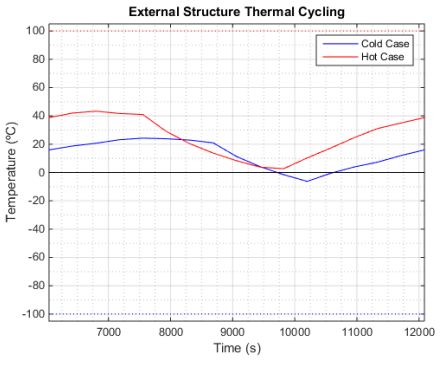

(d) External Structure Thermal Cycling

Figure 13: Thermal cycling after developing the thermal control system

It can be verified that the fundamental frequency increased significantly as a consequence of adding the stainless steel plates to the PCB stack. The resulting mode of vibration is presented in Figure 14.

5. Conclusions

ECOSat-III dynamic and thermal behaviour were simulated and analysed. Only a partial model was experimentally tested and design changes were made by the ECOSat team after testing that par-

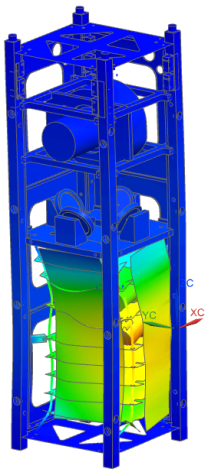

Figure 14: First mode shape after applying the thermal control system

tial model. Because of that, the computational model was changed to correspond to the tested model. The FEM model had to be updated to match the simulated results with the experimental ones. These results did not comply with the requirements because the fundamental frequency of the satellite was below the minimum required value. Before proposing a solution, the effect of changing the satellite configuration to its final configuration was evaluated and it was concluded that the results were close to the results of the tested configuration. Since the tested configuration will not be used in the future, it was abandoned and the final configuration was used to obtain a solution to increase the fundamental frequency. The proposed solution was to add two aluminum parts to constrain the first mode of vibration, increasing the fundamental frequency.

To guarantee a good thermal behaviour, the worst case conditions in terms of minimum temperatures and maximum temperatures were identified, the components that reached temperatures beyond the safe range were identified and a passive thermal control system was developed. Since the non-safe temperatures occurred in the cold case, it was proposed to use black colours in the external surfaces of the satellite and to isolate the camera from the external structure by changing the material of one of its mounting plates. With this procedure, all the components operate in their safe temperature range. An additional design change was suggested. It consisted in adding high thermal inertia plates to the electronics stack and change the remaining mounting plates to stainless steel. This changes reduced the maximum temperature and temperature deltas in hot case conditions. A new modal analysis confirmed that the fundamental frequency and solid properties were still within the required limits.

Acknowledgements

I would like to thank my supervisor Dr. Afzal Suleman for providing me the opportunity to work in Centre for Aerospace Research in University of Victoria and for the financial support during my stay in Canada. I would like to thank the ECOSat team for helping me whenever I needed. I would like to give a special thanks to Cass Hussmann for all the orientation he provided during the development of my work and to Abdul Fourteia who showed himself very helpful at all times. I would also like to thank Stephen Warwick and Peter Sherk from Centre for Aerospace Research in Victoria International Airport who managed to provide me a work station with all the resources I needed. I want to thank all the members of the Centre for Aerospace Research, in both University of Victoria and Victoria International Airport, and of the ECOSat team for the amazing experience in Canada.

I would like to thank my colleagues and professors I met during my Aerospace Engineering course who helped me surpass my limits.

Last but not least, I would like to thank my mother, grandmother and brother for the unconditional support during my journey.

References

[1] D. DePasquale and J. Bradford. Nano/Microsatellite Market Assessment. SpaceWorks Enterprises Inc., 2014. Retrieved from http://spaceworksforecast.com/.

[2] M. N. Sweeting. Keynote Address: Micro/Nanosatellites The New World. In *Smaller Satellites: Bigger Business?*, volume 6, pages 1–19. Springer, 2002.

[3] S. Lee, A. Hutputanasin, A. Toorian, W. Lan, and R. Munakata. *CubeSat Design Specification, Revision 13.* California Polytechnic State University, 2015.

[4] S. S. Rao and F. F. Yap. *Mechanical Vibrations.* Addison-Wesley New York, 1995.

[5] P. Avitabile. Experimental Modal Analysis. *Journal of Sound and Vibration*, 35(1):20–31, 2001.

[6] Dynamic Design Solutions NV. *FEMtools Model Updating Theoretical Manual.* FEMtools Documentation, 2015.

[7] T. L. Bergman, F. P. Incropera, D. P. DeWitt, and A. S. Lavine. *Fundamentals of Heat and Mass Transfer.* John Wiley & Sons, 2011.